

Article

Effect of Tool Rotational Speed on the Microstructure and Mechanical Properties of Bobbin Tool Friction Stir Welded 6082-T6 Aluminum Alloy

Yupeng Li ^{1,2,3,4,*}, Daqian Sun ^{1,2} and Wenbiao Gong ^{3,4}

¹ Key Laboratory of Automobile Materials, Ministry of Education, Jilin University, Changchun 130025, China

² School of Materials Science and Engineering, Jilin University, Changchun 130025, China

³ Key Laboratory of Advanced Structural Materials, Ministry of Education, Changchun University of Technology, Changchun 130012, China

⁴ School of Materials Science and Engineering, Changchun University of Technology, Changchun 130012, China

* Correspondence: lyp.ccut@163.com; Tel.: +86-155-2663-9851

Received: 10 July 2019; Accepted: 13 August 2019; Published: 15 August 2019



Abstract: Samples of 6082-T6 aluminum alloy were welded by bobbin tool friction stir welding at different rotational speeds. The thermal cycles, microstructure, microhardness, and tensile properties of the specimens were investigated. The results show that the maximum temperature at the joint increases first and then decreases with increasing rotational speed, and the maximum temperature is 509 °C at 1000 r/min. The macromorphology of the cross-section of the joint is rectangular, and an “S” line and gray-white texture can be observed. The stirred zone had much smaller equiaxed recrystallized grains. With increasing welding speed, the average grain size in the stirred zone region decreases. The microhardness distribution of the cross-section of all joints is W-shaped. When the rotational speed increases, the hardness of the heat-affected zone decreases gradually, and the hardness of the stirred zone increases. At 600 r/min, the strength is the lowest. The fracture location is between the stirred zone and the thermomechanically affected zone. When the rotational speed is increased, the fracture location is entirely located in the heat affected zone, and the fracture surface is dimple-like; the strength significantly increases and reaches a maximum at 800 r/min.

Keywords: bobble tool friction stir welding; 6082-T6 aluminum alloy; rotational speed; microstructure; mechanical properties

1. Introduction

Friction stir welding (FSW) is a solid-state joining process originally intended for aluminum alloys and developed by The Welding Institute (TWI) in 1991 [1–3]. Because the metal material is not melted during the FSW process, the welding joint has small shrinkage deformation, and the loss of mechanical properties is obviously reduced compared with traditional welding techniques [4–6]. Bobbin tool friction stir welding (BT-FSW) is a variant type of FSW that employs a bottom shoulder to contact the bottom surface of the work piece [7]. There is no need for a backing bar because the BT-FSW allows for less stiffness during the welding process, and closed profiles, such as hollow and complex-shaped structures, can be joined [8].

To date, several studies have been conducted to evaluate the temperature field [9,10], equipment [11], microstructures and mechanical properties [12–15] of bobbin tool friction stir welded joints in aluminum alloys. The microstructure and the mechanical properties are determined by the thermal cycle and the material flow behavior for the FSW [16]. The welding parameters, including the rotational speed and welding speed, have an obvious effect on the thermal cycle and the material

flow behavior. Li et al. [17] studied the effects of rotational and welding speeds on the microstructure and mechanical properties of BT-FSW Mg AZ31 and indicated that the average grain size increased as the ratio of the rotational speed to welding speed increased and the rotational and welding speeds had only slight influences on the yield stress and fracture elongation. Wang et al. [18] noted that the tensile strength of the BT-FSW joint welded Al-Li alloy initially increased with rotational speed and then decreased, with the maximal strength efficiency reaching 80%. Liu et al. [19] studied the effect of welding speed on the microstructure and mechanical properties of BT-FSW welded 6061-T6 aluminum alloy and found that the elongation and tensile strength of joints increased with increasing welding speed. Zhang et al. [20] concluded that with increasing welding speed, the joint of the BT-FSW joint welded 2A14-T6 aluminum alloy strength first increased to a peak and then showed a sharp decrease due to the occurrence of void defects. Wang et al. [21] studied the dual-rotation bobbin tool friction stir welding (DBT-FSW) on Al-Li alloy sheets and found that the DBT-FSW has an excellent process stability and can produce the defect-free joints in a wider range of welding parameters. Zhao et al. [22] developed empirical models to describe the relationships between the welding factors, such as welding speed, tool rotation speed, and shoulder pinching gap, and the tensile properties of BT-FSW 2219-T87 aluminum alloy, and the result shows that the models are adequate for predicting and optimizing the BT-FSW factor effects.

In summary, although some studies on BT-FSW process parameters have been carried out in recent years, there is little work on the effect of rotational speed on the microstructure and mechanical properties of BT-FSW of 6000 series aluminum alloys, especially in 6082-T6 aluminum alloys. The main purposes of this study are to investigate the application of BT-FSW on 6082-T6 aluminum alloy and to determine the effect of rotational speed on the microstructure and mechanical properties of the obtained joints.

2. Materials and Methods

The base metal (BM) used in this study was 6082-T6 aluminum alloy with a thickness of 4 mm in plate form. The size of the test plates used for the welding experiment was 500 mm × 150 mm × 4 mm. The chemical composition and mechanical properties of the BM are presented in Table 1.

Table 1. Chemical composition and mechanical properties of 6082-T6 aluminum alloy.

Chemical Composition (wt%)								Mechanical Properties			
Si	Fe	Cu	Mn	Mg	Cr	Zn	Ti	Al	Tensile Strength	Yield Strength	Elongation
0.97	0.50	0.10	0.7	1.02	0.25	0.20	0.10	Bal	323 MPa	272 MPa	13%

The test plates were butt-welded by the BT-FSW method with a special FSW Machine (FSW-LM-AM16, AVIC Beijing FSW Technology Co., Ltd., Beijing, China). The welding tool consisted of two shoulders with 16 mm diameters and a smooth cylindrical pin 6 mm in diameter and 3.8 mm in length, as shown in Figure 1; the shoulders and the pin are all made of steel H13. During welding, the welding tool, with a tilting angle of 0°, was rotated in the clockwise direction; the welding speed was 500 mm/min constantly, and the rotational speeds of the tool were 600 r/min, 800 r/min, 1000 r/min and 1200 r/min.

The thermal cycle curves of different positions on both sides of the weld were measured by a Digital Recorder (RX4008BJL, Hangzhou Excon Technology Co., Ltd., Hangzhou, China) and several thermocouples. The thermocouples were K-type armored thermocouples with a diameter of 1 mm, and the installation method is shown in Figure 2. Samples for microstructure analysis were cut perpendicular to the welding direction, mechanically ground and polished, etched with a reagent (20 g NaOH and 100 mL H₂O), and examined by Optical Microscopy (DMI3000M, Leica Microsystems Inc., Wetzlar, Germany). Electron Backscattered Diffraction (EBSD, Tescan Vega3, Tescan Orsay Holding,

Brno, Czech Republic) was also used to study the microstructure. The fracture surface was observed by Scanning Electron Microscopy (SEM, JSM-5600, JEOL Ltd., Tokyo, Japan).

The microhardness was measured along the cross-section of the joint using an FM-800 Microhardness (Future-Tech Corp. Kanagawa, Kawaki, Japan) instrument with a test load of 100 g and an indentation time of 15 s. Measurements were performed pointwise at the center of the thickness at 0.5 mm intervals. Tensile samples were machined from the middle parts of the weld, as shown in Figure 3, with a gauge 50 mm long and 12.5 mm wide according to ASTM E8/E8M-13a [23], and tensile tests for each condition were performed in triplicate. The tensile properties were tested with a WDW-200 Tensile Testing Machine (Changchun Kexin Test Instrument Co., Ltd., Changchun, China) at room temperature and at a testing speed of 1 mm/min.

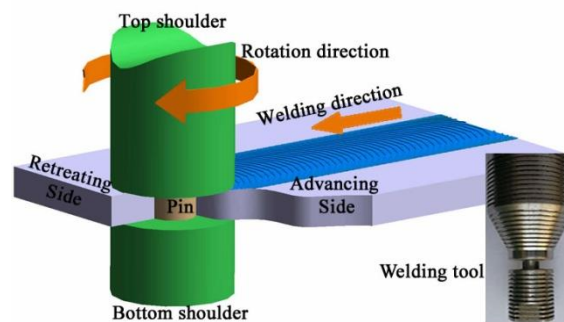


Figure 1. Schematic illustration of the bobbin tool friction stir welding (BT-FSW) process.

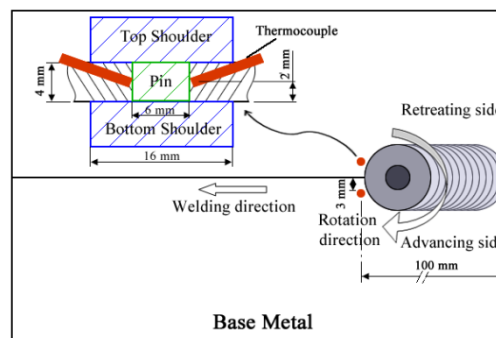


Figure 2. Schematic illustration of the test method for the thermal cycle curve.

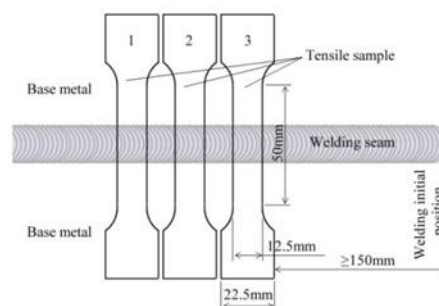


Figure 3. Schematic illustration of the tensile sample.

3. Results

3.1. Welding Thermal Cycles

In the BT-FSW process, the friction heat produced by friction between the BT-FSW tool and the workpiece and the deformation heat produced by severe plastic deformation in the zone around the stirring pin will cause the temperature in the stirring zone and its vicinity to rise rapidly. The distribution

of the temperature field around the stirring zone not only affects the plastic flow of the material but also directly affects the microstructure of different regions of the welded joint, such as the grain size, precipitation coarsening and dissolution of the second phase. Furthermore, the mechanical properties and welding quality of the joints are affected. Figure 4 shows the effect of different rotational speeds on the recorded welding thermal cycles. As the rotational speed increases from 600 r/min to 1000 r/min, the peak temperature of the retreating side increases from 463 °C to 509 °C. When the speed reached 1200 r/min, the maximum temperature fell back to 491.5 °C.

The heat production of FSW is related to the rotational speed of the tool, yield shear stress, friction coefficient, contact pressure between the tool and the matrix, etc. For the aluminum alloy, the yield strength decreases with increasing temperature, so the yield shear stress, contact pressure and friction coefficient will decrease with increasing temperature. Therefore, when the rotational speed of the tool is increased, although the heat production may be increased and the temperature will rise, the yield shear stress, contact pressure and friction coefficient will decrease with increasing temperature, which will lead to a decrease in the actual heat production. Because of this, FSW can keep the base metal in the solid state for welding.

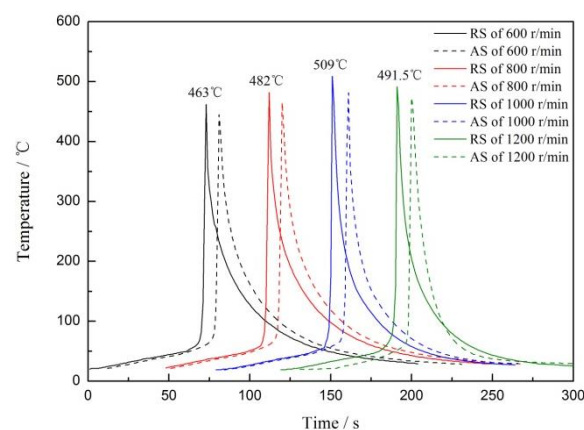


Figure 4. Welding thermal cycle curves at different rotational speeds. RS: retreating side; AS: advancing side.

It can also be seen in Figure 4 that the maximum temperature of each rotation at the retreating side (RS) of the welded joint is higher than the advancing side (AS), and the temperature difference is approximately 20 °C. In the BT-FSW, with the rotation of the tool, the shoulder and the pin not only produce heat by friction but also drive the plastic metals on the upper and lower surfaces of the plate and the weld nugget area to rotate from the AS of the tool to the RS. At the same time, heat transfer occurs when the plastic metals transfer. In addition, in the stir zone (SZ) and thermomechanically affected zone (TMAZ) of the friction stir welding joint, the welded metal undergoes severe plastic deformation, resulting in plastic deformation heat. The deformation and strain rate of the metal on the RS are higher than those on the AS, and the heat of plastic deformation produced by the metal on the RS is higher than that on the AS, so the temperature on the RS is higher than that on the AS.

3.2. Microstructure of the Joints

The macromorphology of the joints after welding is shown in Figure 5. The surfaces of the joint have no disfigurement, the weld ripple is arranged regularly, and there are a few flying edges on both sides of the weld. Comparing the weld ripple with different rotating speeds, the distance between the ripples is shortened when the rotating speed is increased. Measurements of ripple spacing values are shown in Table 2. The ripple spacing corresponds to the ratio of the forward speed and rotational speed of the tool, which is approximately equal to the forward distance of the tool in each circle of rotation.

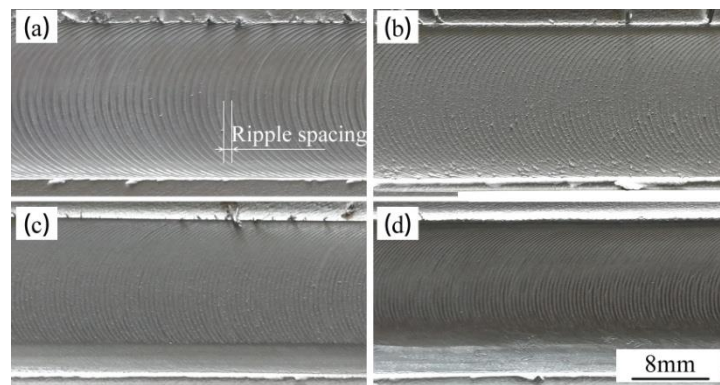


Figure 5. Macromorphology of the weld surface at different rotational speeds.

Table 2. The distance of the weld ripple at different rotational speeds.

No.	Welding Speed (mm/min)	Rotational Speed (r/min)	Distance of Ripple (mm)	The Distance Per Revolution of the Tool (mm)
1	500	600	0.82	0.833
2	500	800	0.61	0.625
3	500	1000	0.5	0.5
4	500	1200	0.41	0.417

Low magnification optical macrographs of the cross-section of BT-FSW joints as the rotational speed varied from 600 to 1200 r/min are shown in Figure 6. With respect to conventional FSW, all the joints exhibit four distinctive zones between the AS and the RS, i.e., the BM, heat-affected zone (HAZ), thermomechanically affected zone (TMAZ), and stir zone (SZ), as depicted in Figure 6a.

As shown in Figure 6, the black line at the center of the SZ is the “S” line. According to Sato and coworkers, in the as-welded condition, the “S” line is composed of broken oxide particles, and these broken oxide particles disperse along the fine equiaxed grain boundaries [24]. Zhang et al. [25] concluded that the “S” line originated from the oxide film on the initial butting surfaces and experienced only the thermomechanical deformation process without a change in the chemical composition. The morphologies of the segregation bands and the “S” line were dependent on the welding parameters.

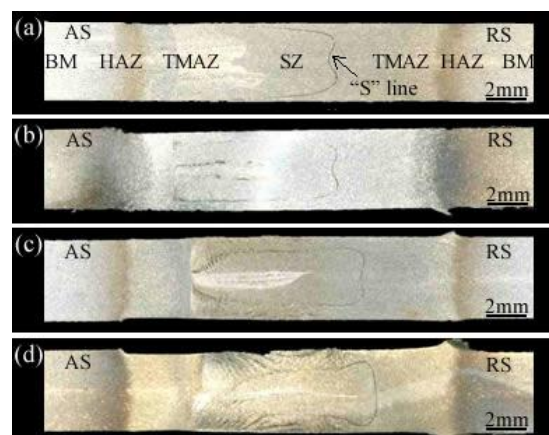


Figure 6. Cross-sections of BT-FSW joints welded for different rotational speeds: (a) 600 r/min, (b) 800 r/min, (c) 1000 r/min and (d) 1200 r/min. BM: base metal; HAZ: heat-affected zone; TMAZ: thermomechanically affected zone; SZ: stir zone.

Figure 7a shows the “S” line schematic diagram of welded joints at different rotational speeds. From the diagram, it can be seen that the S-line presents an opposite “C” shape, opening on the AS side and closing on the RS side. With the increase of the rotational speed, the “S” line gradually extends to both sides, and the height becomes narrower. In BT-FSW, the plastic metal located in front of the tool will be driven by the shoulders and pin and transferred to the gap formed by the advance of the tool behind the stirring needle, thus forming a weld, as shown in Figure 7b. When the rotation speed is 600 r/min, the distance per revolution of the tool is 0.833 mm, the clearance formed by the tool of the agitator is large, and the molding metal of the butt surface can be transferred to a longer distance. The distance per revolution of the tool decreases to 0.417 mm when the rotating speed increases to 1200 r/min, so the plastic metal is transferred closer, and butting surfaces are only transferred to the side of the stirring needle.

Series of light and dark stripes can be observed in the SZ, as shown in Figure 6. In friction stir welding, high temperature plastic metals are stirred, extruded and formed under the action of upper and lower shoulders and pins. The original oxide on the surface and side of the specimen is stirred and broken, and other plastic metals are mixed and transferred to the back of the pin; eventually, the bright and dark stripes in the weld are formed. When the stirring speed increases, the stirring intensity increases, and the texture becomes more obvious. At the same time, due to the increase of stirring speed, the heat input of joints increases, and more Al matrix is oxidized rapidly during welding, which makes the texture more pronounced.

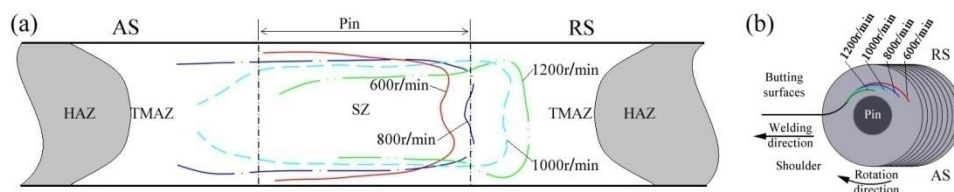


Figure 7. Schematic diagram of: (a) the “S” line morphology of the section at different rotational speeds, (b) the flow process of plastic metal.

Figure 8 shows the microstructure of the grain morphologies of the different zones in the joint at 1200 r/min. Compared with the elongated coarse and fine grained areas of the BM, as shown in Figure 8a, the SZ, as shown in Figure 8d, has much smaller equiaxed recrystallized grains. Under the action of the pin, the SZ produced a large plastic deformation and formed new grain boundaries and a higher density of dislocations. Recrystallization occurred at the same time and was formed of uniform fine equiaxed crystals. Because of the stirring shear effect of the mechanical rotation of the shoulder and the pin, the grains of the TMAZ, as shown in Figure 8c,e, were transformed to bending and elongated grains. Due to the effect of thermal cycling, some grains recrystallized and have a more uniform grain size distribution on the basis of the rolling morphologies of the BM in the HAZ, as shown in Figure 8b,f, and the average grain size of HAZ has increased.

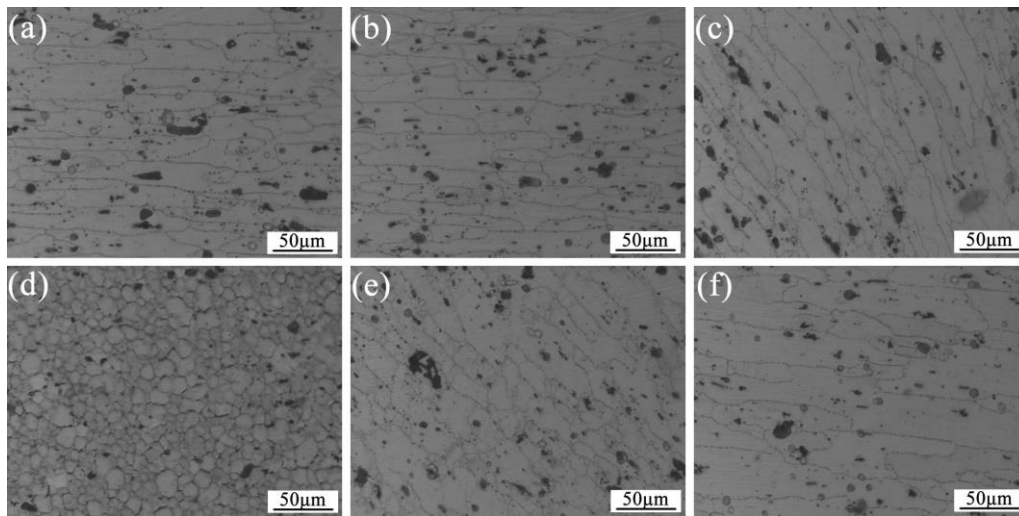


Figure 8. Microstructures viewed with an optical microscope of the joint at 1200 r/min: (a) BM, (b) HAZ on AS, (c) TMAZ on AS, (d) SZ, (e) TMAZ on RS and (f) HAZ on RS.

Figure 9 shows the EBSD micrographs of SZ at different rotational speeds. It can be seen from the micrographs that the rotational speed increases from 600 r/min to 1200 r/min, and the average grain size in SZ decreases from 9.7 μm to 7.1 μm , as shown in Table 3. It is generally believed that during FSW, the microstructures in the SZ will undergo complex evolution processes, such as discontinuous dynamic recrystallization, dynamic recovery and grain growth, continuous dynamic recrystallization, and grain coarsening [26]. When the metal is stirred directly by the pin, severe plastic deformation will occur, and a large number of dislocations will form. The stress imbalance in the high-density dislocation region results in the local migration of grain boundaries and protrusions. These protrusions are cut and broken in subsequent deformation, resulting in a large number of fine nuclei. These nuclei gradually coarsen and grow under the action of friction heat and eventually form equiaxed crystals. In this experiment, the temperature difference caused by the change of rotating speed is not large, but the degree of deformation and dynamic recrystallization caused by rotating speed is greater, so the grain size decreases with the increase of rotating speed.

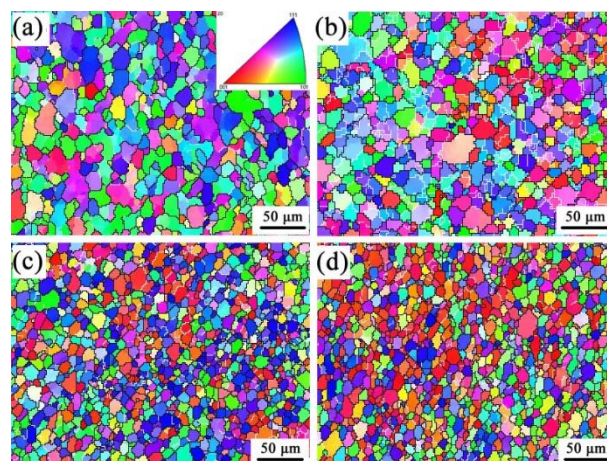


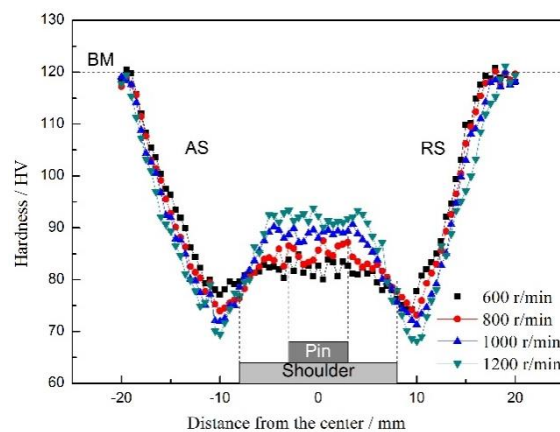
Figure 9. Electron backscattered diffraction (EBSD) micrographs of the SZ obtained at different rotational speeds: (a) 600 r/min, (b) 800 r/min, (c) 1000 r/min and (d) 1200 r/min.

Table 3. Grain size in SZ at different rotational speeds.

Rotation Speed (r/min)	Average Grain Size/ μm
600	9.1
800	8.5
1000	7.4
1200	7.1

3.3. Mechanical Properties of the Joints

Figure 10 shows the variation in the microhardness along the mid-thickness of the joints at different rotational speeds. It can be seen from the diagram that with respect to the BT-FSW joints, all the microhardness distribution profiles exhibit a W-shape. The minimum hardness appeared in the HAZ and was HV 68–74, and it rose to HV 80–94 at the center of the SZ. The hardness of the BM was highest, with an average value of HV 120.

**Figure 10.** Microhardness distribution of the joints welded at different rotational speeds.

With the rotational speed increasing from 600 r/min to 1200 r/min, the hardness of the SZ increased. When the speed increases, the average grain size in SZ decreases, and the dislocation density increases, which leads to an increase in microhardness. With the increase of rotational speed, the hardness of the HAZ adjacent to the TMAZ tends to decrease. According to [13,27], this is mainly attributed to the dissolution and precipitation of the second phase and the change of the grain size of the aluminum matrix in the microstructure of the zone. With the increase of rotational speed, the heat input and peak temperature increase obviously, which promotes the dissolution of the β'' phase and the precipitation and growth of the β' phase. Moreover, the grain size of the aluminum matrix is coarser, which leads to a reduction in the hardness of the HAZ.

The tensile properties of the joints welded at different rotational speeds are shown in Figure 11. The graph shows that the lowest tensile strength at 600 r/min is 197.7 MPa. The maximum tensile strength is 262.7 MPa at a rotational speed of 800 r/min. The elongation reached a maximum at 1000 r/min, which was 8.3%. Figure 12 shows the typical fracture location of joints produced at different rotational speeds. The fracture locations of 600 r/min were found at the border of the SZ and the TMAZ of AS and that of 800 r/min to 1200 r/min in the HAZ of AS.

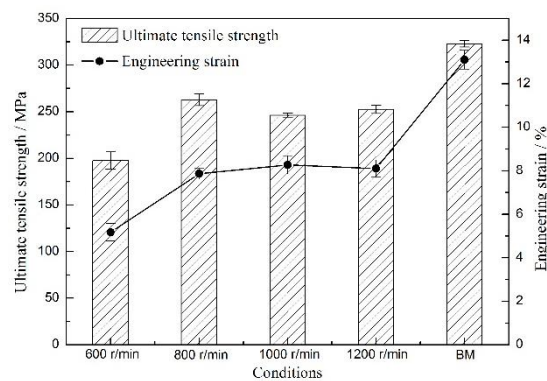


Figure 11. Tensile properties of the joints at different rotational speeds.



Figure 12. Typical fracture location of joints at different rotation speeds: (a) 600 r/min; (b) 800 r/min.

The fracture surfaces of all specimens were analyzed by scanning electron microscopy (SEM), as shown in Figure 13. When the rotating speed is 600 r/min, the heat input is low, the dynamic recrystallization in the SZ region is low and the grain size is large. In addition, the relative displacement of the tool is the largest in each rotating circle, and the extrusion force of the tool on the metal transferred by stirring decreases, which results in the fracture of the weak area between SZ and TMAZ. Fracture morphology, as shown in Figure 13a, shows that this type of fracture presents a large number of small and shallow dimples with layered distribution, which belongs to a ductile fracture.

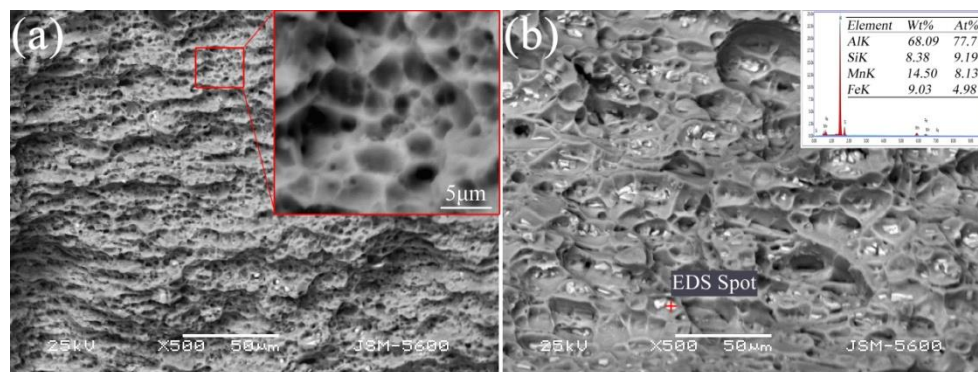


Figure 13. Typical fracture surfaces of joints at different rotation speeds: (a) 600 r/min, (b) 800 r/min.

When the rotation speed increases to more than 800 r/min, the SZ is stirred sufficiently, and the fine grains formed by dynamic recrystallization improve the strength of this zone. However, with increasing heat input, the strengthened phase dissolves, and the grain size increases in the HAZ. As a result, the strength and hardness of the region are reduced. When the load is applied and reaches the yield strength, the HAZ will yield and deform first. It may be because of the different work hardening exponents of the HAZ under stress that the joint breaks in the HAZ on AS during tension. The fracture morphology of Figure 13b shows that the fracture of HAZ is mainly dimple fractures, with large and shallow dimples and white AlFeMnSi second-phase particles at the bottom.

4. Conclusions

In this paper, 6082-T6 aluminum alloy was successfully welded by BT-FSW using different rotation speeds. The typical microstructures and mechanical properties of every joint were investigated. The main conclusions can be summarized as follows.

1. The maximum temperature at the joint increases first and then decreases with increasing rotational speed, reaching a maximum temperature of 509 °C at 1000 r/min. The maximum temperature at the RS of the joints is higher than the AS, and the temperature difference is approximately 20 °C.
2. The macromorphology of the cross-section of the joint is rectangular, and an “S” line and gray-white texture can be observed. The “S” line is an opposite “C” shape, and the opening is on the AS side. With increasing welding speed, the “S” line is elongated and narrowed.
3. In the welded joint, the SZ has much smaller equiaxed recrystallized grains, and the TMAZ are elongated to form bending and elongated grains. In the HAZ, some grains are recrystallized and have a better grain size uniformity based on the rolling morphologies of BM. With increasing welding speed, the average grain size in the SZ region decreases from 9.1 micron to 7.1 micron.
4. The joints present a W-shaped hardness profile along their cross-section. The minimum hardness appears in the HAZ and is HV 68–74, rising to HV 80–94 at the center of the SZ. When the rotational speed increases from 600 r/min to 1200 r/min, the hardness of HAZ decreases gradually, and the hardness of SZ increases.
5. When the rotational speed is 600 r/min, the strength is the lowest. The fracture location between SZ and TMAZ. When the rotational speed is increased, the fracture location is all in HAZ, and the fracture surface is dimple-like. The ultimate tensile strength significantly increases and reaches a maximum (262.7 MPa) at 800 r/min; the engineering strain is 7.9%.

Author Contributions: Conceptualization, W.G. and Y.L.; methodology, Y.L.; investigation, Y.L.; writing—original draft preparation, Y.L.; writing—review and editing, Y.L. and W.G.; supervision, D.S.

Funding: This research received no external funding.

Conflicts of Interest: The authors declare no conflict of interest.

References

1. Thomas, W. Friction Stir Welding. International Patent Application No PCT/GB92/02203, 6 December 1991.
2. Dialami, N.; Cervera, M.; Chiumenti, M. Effect of the tool tilt angle on the heat generation and the material flow in friction stir welding. *Metals* **2019**, *9*, 28. [[CrossRef](#)]
3. Hamilton, C.; Dymek, S.; Kopyscianski, M.; Weglowska, A.; Pietras, A. Numerically based phase transformation maps for dissimilar aluminum alloys joined by friction stir-welding. *Metals* **2018**, *8*, 324. [[CrossRef](#)]
4. Nandan, R.; DebRoy, T.; Bhadeshia, H.K.D.H. Recent advances in friction-stir welding—Process, weldment structure and properties. *Prog. Mater. Sci.* **2008**, *53*, 980–1023. [[CrossRef](#)]
5. Hamilton, C.; Dymek, S.; Sommers, A. Characteristic temperature curves for aluminum alloys during friction stir welding. *Weld. J.* **2010**, *89*, 189–194.
6. Bussu, G.; Irving, P.E. The role of residual stress and heat affected zone properties on fatigue crack propagation in friction stir welded 2024-T351 aluminium joints. *Int. J. Fatigue* **2003**, *25*, 77–88. [[CrossRef](#)]
7. Threadgill, P.L.; Ahmed, M.M.Z.; Martin, J.P.; Perrett, J.G.; Wynne, B.P. The use of bobbin tools for friction stir welding of aluminium alloys. *Mater. Sci. Forum* **2010**, *638–642*, 1179–1184. [[CrossRef](#)]
8. Huang, Y.X.; Wan, L.; Lv, S.X.; Feng, J.C. Novel design of tool for joining hollow extrusion by friction stir welding. *Sci. Technol. Weld. Joining* **2013**, *18*, 239–246. [[CrossRef](#)]
9. Li, J.Y.; Zhou, X.P.; Dong, C.L.; Dong, J.H. Temperature fields in 6082 aluminum alloy samples bobbin-tool friction stir welded. *J. Aeronaut. Mater.* **2013**, *33*, 36–40.
10. Liu, X.M.; Yao, J.S.; Cai, Y.; Meng, H.; Zou, Z.D. Simulation on the temperature field of bobbin tool friction stir welding of AA 2014 aluminium alloy. *Appl. Mech. Mater.* **2013**, *433–435*, 2091–2095. [[CrossRef](#)]
11. Chen, S.J.; Li, H.; Lu, S.; Ni, R.Y.; Dong, J.H. Temperature measurement and control of bobbin tool friction stir welding. *Int. J. Adv. Manuf. Technol.* **2016**, *86*, 337–346. [[CrossRef](#)]

12. Wan, L.; Huang, Y.X.; Lv, Z.L.; Lv, S.X.; Feng, J.C. Effect of self-support friction stir welding on microstructure and microhardness of 6082-T6 aluminum alloy joint. *Mater. Des.* **2014**, *55*, 197–203. [[CrossRef](#)]
13. Li, Y.P.; Sun, D.Q.; Gong, W.B.; Liu, L. Effects of postweld aging on the microstructure and properties of bobbin tool friction stir-welded 6082-T6 aluminum alloy. *Int. J. Miner. Metall. Mater.* **2019**, *26*, 849–857. [[CrossRef](#)]
14. Dong, J.H.; Gao, C.; Lu, Y.; Han, J.; Jiao, X.D.; Zhu, Z.X. Microstructural characteristics and mechanical properties of bobbin-tool friction stir welded 2024-T3 aluminum alloy. *Int. J. Miner. Metall. Mater.* **2017**, *24*, 171–178. [[CrossRef](#)]
15. Okamoto, K.; Sato, A.; Park, S.H.; Hirano, S. Microstructure and Mechanical Properties of FSWed Aluminum Extrusion with Bobbin Tools. *Mater. Sci. Forum* **2012**, 706–709, 990–995. [[CrossRef](#)]
16. Mahmoud, T.S.; Gaafer, A.M.; Khalifa, T.A. Effect of tool rotational and welding speeds on microstructural and mechanical characteristics of friction stir welded A319 cast Al alloy. *Metal. Sci. J.* **2008**, *24*, 553–559. [[CrossRef](#)]
17. Li, W.Y.; Fu, T.; Hütsch, L.; Hilgert, J.; Wang, F.F.; dos Santos, J.F.; Huber, N. Effects of tool rotational and welding speed on microstructure and mechanical properties of bobbin-tool friction-stir welded Mg AZ 31. *Mater. Des.* **2014**, *64*, 714–720.
18. Wang, F.F.; Li, W.Y.; Shen, J.J.; Hu, S.Y.; Dos Santos, J.F. Effect of tool rotational speed on the microstructure and mechanical properties of bobbin tool friction stir welding of Al-Li alloy. *Mater. Des.* **2015**, *86*, 933–940. [[CrossRef](#)]
19. Liu, H.J.; Hou, J.C.; Guo, H. Effect of welding speed on microstructure and mechanical properties of self-reacting friction stir welded 6061-T6 aluminum alloy. *Mater. Des.* **2013**, *50*, 872–878. [[CrossRef](#)]
20. Zhang, H.J.; Wang, M.; Zhang, X.; Yang, G.X. Microstructural characteristics and mechanical properties of bobbin tool friction stir welded 2A14-T6 aluminum alloy. *Mater. Des.* **2015**, *65*, 559–566. [[CrossRef](#)]
21. Wang, F.F.; Li, W.Y.; Shen, J.; Wen, Q.; dos Santos, J.F. Improving weld formability by a novel dual-rotation bobbin tool friction stir welding. *J. Mater. Sci. Technol.* **2018**, *34*, 135–139. [[CrossRef](#)]
22. Zhao, S.; Bi, Q.Z.; Wang, Y.H.; Shi, J. Empirical modeling for the effects of welding factors on tensile properties of bobbin tool friction stir-welded 2219-T87 aluminum alloy. *Int. J. Adv. Manuf. Technol.* **2018**, *90*, 1105–1118. [[CrossRef](#)]
23. ASTM E8/E8M-13a. *Standard Test Methods for Tension Testing of Metallic Materials*; ASTM International: West Conshohocken, PA, USA, 2013.
24. Sato, Y.S.; Takauchi, H.; Park, S.H.C.; Kokawa, H. Characteristics of the kissing-bond in friction stir welded Al alloy 1050. *Mater. Sci. Eng. A* **2005**, *405*, 333–338. [[CrossRef](#)]
25. Zhang, Z.; Xiao, B.L.; Ma, Z.Y. Effect of segregation of secondary phase particles and “S” line on tensile fracture behavior of friction stir-welded 2024Al-T351 joints. *Metall. Mater. Trans. A* **2013**, *44A*, 4081–4097. [[CrossRef](#)]
26. Su, J.Q.; Nelson, T.W.; Sering, C.J. Microstructure evolution during FSW/FSP of high strength aluminum alloys. *Mater. Sci. Eng. A* **2005**, *405*, 277–286. [[CrossRef](#)]
27. Dong, P. Study on microstructures and properties of friction stir welding joints of 6005A-T6 aluminum alloy. Ph.D. Thesis, Jilin University, Changchun, China, 4 June 2014.

